Journal of Zhejiang University SCIENCE A
ISSN 1673-565X (Print); ISSN 1862-1775 (Online)
www.zju.edu.cn/jzus; www.springerlink.com
E-mail: jzus@zju.edu.cn

Dynamic modeling and direct power control of wind turbine driven DFIG under unbalanced network voltage conditions*

Jia-bing HU†1, Yi-kang HE[1], Lie XU[2]

([1]*School of Electrical Engineering, Zhejiang University, Hangzhou 310027, China*)

([2]*Department of Electronics and Electrical Engineering, University of Strathclyde, Glasgow G4 0PG, UK*)

†E-mail: emec_zju@zju.edu.cn

Received Apr. 18, 2008; revision accepted July 3, 2008; CrossCheck deposited Nov. 10, 2008

Abstract: This paper proposes an analysis and a direct power control (DPC) design of a wind turbine driven doubly-fed induction generator (DFIG) under unbalanced network voltage conditions. A DFIG model described in the positive and negative synchronous reference frames is presented. Variations of the stator output active and reactive powers are fully deduced in the presence of negative sequence supply voltage and rotor flux. An enhanced DPC scheme is proposed to eliminate stator active power oscillation during network unbalance. The proposed control scheme removes rotor current regulators and the decomposition processing of positive and negative sequence rotor currents. Simulation results using PSCAD/EMTDC are presented on a 2-MW DFIG wind power generation system to validate the feasibility of the proposed control scheme under balanced and unbalanced network conditions.

Key words: Doubly-fed induction generator (DFIG), Wind turbine, Direct power control (DPC), Stator voltage oriented (SVO), Unbalanced network

doi:10.1631/jzus.A0820297 **Document code:** A **CLC number:** TM315; TM614

INTRODUCTION

Wind farms based on the doubly-fed induction generators (DFIGs) with converters rated at 25%~30% of the generator rating for a given rotor speed variation range of ±25% are becoming increasingly popular. Compared with the wind turbines using fixed speed induction generators or fully-fed synchronous generators with full-size converters, the DFIG-based wind turbines offer not only the advantages of variable speed operation and four-quadrant active and reactive power capabilities, but also lower converter cost and power losses (Pena *et al*., 1996). However, both transmission and distribution networks could usually have small steady state and large transient voltage unbalance. If voltage unbalance is not considered by the DFIG control system, the stator current could become highly unbalanced even with a small unbalanced stator voltage. The unbalanced currents create unequal heating on the stator windings, and pulsations in the electromagnetic torque and stator output active and reactive powers (Chomat *et al*., 2002; Jang *et al*., 2006; Zhou *et al*., 2007; Pena *et al*., 2007; Hu *et al*., 2007; Xu and Wang, 2007; Hu and He, 2008).

Control and operation of DFIG wind turbine systems under unbalanced network conditions is traditionally based on either stator-flux-oriented (SFO) (Xu and Wang, 2007) or stator-voltage-oriented (SVO) vector control (Jang *et al*., 2006; Zhou *et al*., 2007; Hu *et al*., 2007; Hu and He, 2008). The scheme in (Jang *et al*., 2006; Zhou *et al*., 2007; Xu and Wang, 2007; Hu *et al*., 2007) employs dual-PI (proportional integral) current regulators implemented in the positive and negative synchronously rotating reference frames, respectively, which has to decompose the measured rotor current into positive and negative

* Project (No. 50577056) supported by the National Natural Science Foundation of China

sequence components to control them individually. One main drawback of this approach is that, the time delays introduced by decomposing the sequential components of rotor current can affect the overall system stability and dynamic response. Thus, a current control scheme based on a proportional resonant (PR) regulator in the stator stationary reference frame was proposed in (Hu and He, 2008), which can directly control the rotor current without the need of sequential decomposition. Whereas, the performance of the vector control scheme highly depends on the accurate machine parameters such as stator/rotor inductances and resistances used in the control system.

Similar to direct torque control (DTC) of induction machines presented a few decades ago, which behaves as an alternative to vector control, direct power control (DPC) of DFIG-based wind turbine systems has been proposed recently (Gokhale *et al.*, 2002; Xu and Cartwright, 2006; Zhi and Xu, 2007). In (Gokhale *et al.*, 2002), the control scheme was based on the estimated rotor flux. Switching vectors were selected from the optimal switching table using the estimated rotor flux position and the errors of rotor flux and active power. The rotor flux reference was calculated using the reactive power reference. Since the rotor supply frequency, equal to the DFIG slip frequency, might be very low, the rotor flux estimation could be significantly affected by the machine parameter variations. In (Xu and Cartwright, 2006), a DPC strategy based on the estimated stator flux was proposed. As the stator voltage is relatively harmonics-free and fixed in frequency, a DFIG's estimated stator flux accuracy can then be guaranteed. Switching vectors were selected from the optimal switching table using the estimated stator flux position and the errors of the active and reactive powers. Thus, the control system was simple and the machine parameters' impact on the system performance was found to be negligble. However, like a conventional DTC, DPC has the problem of unfixed switching frquency, due to the significant influnce of the active and reactive power variations, generator speed, and power controllers' hysteresis bandwidth. More recently, a modified DPC strategy has been proposed in (Zhi and Xu, 2007) based on SFO vector control in the synchronous reference frame for DFIG-based wind power generation systems with a constant switching frequency. The control method directly calculates the required rotor control voltage within each switching peroid, based on the estimated stator flux, the active and reactive powers and their errors. The control strategy provides improved transient performance with the assumption of the stator (supply) voltage being strictly balanced. However, the operation could be deteriorated during the supply voltage unbalance and there is no report yet on DFIG's DPC under unbalanced network voltage conditions.

This paper investigates an improved DPC scheme for a DFIG wind power generation system under unbalanced network conditions. In the SVO dq^+ reference frame, a mathematical DPC model of a DFIG system with balanced supply is presented, which is referred to as the conventional model in this paper. Then during network unbalance, a modified DFIG's DPC model in the SVO positive dq^+ and negative dq^- reference frames is developed. Based on the developed model, a system control strategy is proposed by eliminating the stator output active power oscillations under unbalanced network conditions. Finally, simulation results on a 2-MW DFIG wind generation system are presented to demonstrate the correctness and feasibility of the proposed control strategy.

DYNAMIC DPC MODEL OF DFIG SYSTEMS

The equivalent circuit of a DFIG in the positive synchronous dq^+ reference frame, rotating at an angular speed of ω_s, is shown in Fig.1.

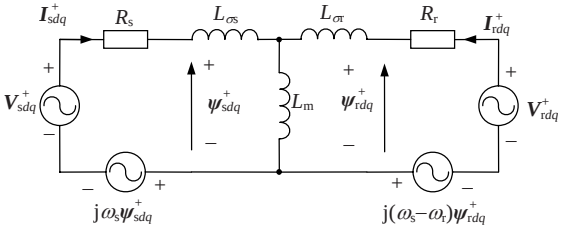

Fig.1 DFIG equivalent circuit in the synchronous dq^+ reference frame

According to Fig.1, the stator and rotor fluxes $\boldsymbol{\psi}^+_{sdq}$ and $\boldsymbol{\psi}^+_{rdq}$ are given by

$$\begin{cases} \boldsymbol{\psi}^+_{sdq} = L_s\boldsymbol{I}^+_{sdq} + L_m\boldsymbol{I}^+_{rdq}, \\ \boldsymbol{\psi}^+_{rdq} = L_r\boldsymbol{I}^+_{rdq} + L_m\boldsymbol{I}^+_{sdq}, \end{cases} \tag{1}$$

where $L_s=L_{\sigma s}+L_m$, $L_r=L_{\sigma r}+L_m$, the superscript '+' refers to the dq^+ reference frame, and L_m, $L_{\sigma s}$ and $L_{\sigma r}$ are the mutual inductance and the stator and rotor leakage inductances, respectively.

From Fig.1, the stator and rotor voltages $\boldsymbol{V}_{sdq}^+$ and $\boldsymbol{V}_{rdq}^+$ are expressed, respectively, by

$$\boldsymbol{V}_{sdq}^+ = R_s\boldsymbol{I}_{sdq}^+ + \frac{\mathrm{d}\boldsymbol{\psi}_{sdq}^+}{\mathrm{d}t} + \mathrm{j}\omega_s\boldsymbol{\psi}_{sdq}^+, \tag{2a}$$

$$\boldsymbol{V}_{rdq}^+ = R_r\boldsymbol{I}_{rdq}^+ + \frac{\mathrm{d}\boldsymbol{\psi}_{rdq}^+}{\mathrm{d}t} + \mathrm{j}\omega_{slip+}\boldsymbol{\psi}_{rdq}^+, \tag{2b}$$

where $\omega_{slip+}=\omega_s-\omega_r$, and ω_r is the rotor angular speed.

Balanced network voltage

A detailed study on the SFO DPC under balanced network conditions was presented in (Zhi and Xu, 2007). This subsection focuses on the modeling of SVO DPC under balanced network conditions, which is recognized as the conventional method in this paper.

Under balanced network conditions, the amplitude and rotating speed of the stator flux are constant. Consequently, in the dq^+ reference frame, the stator flux remains a constant, i.e.,

$$\frac{\mathrm{d}\boldsymbol{\psi}_{sdq}^+}{\mathrm{d}t} = \boldsymbol{0}. \tag{3}$$

Considering Eq.(3) and neglecting the voltage drop across the stator resistance, Eq.(2a) can be simplified as

$$\boldsymbol{V}_{sdq}^+ \approx \mathrm{j}\omega_s\boldsymbol{\psi}_{sdq}^+. \tag{4}$$

As shown in Fig.2, when d-axis of the synchronous frame is fixed to the stator voltage, viz., SVO vector control, Eq.(4) can be rewritten as

$$\psi_{sd}^+ = 0, \quad \psi_{sq}^+ = -V_{sd}^+/\omega_s. \tag{5}$$

According to Eq.(1), the stator current in the dq^+ reference frame is given as

$$\boldsymbol{I}_{sdq}^+ = \frac{L_r\boldsymbol{\psi}_{sdq}^+ - L_m\boldsymbol{\psi}_{rdq}^+}{L_sL_r - L_m^2} = \frac{\boldsymbol{\psi}_{sdq}^+}{\sigma L_s} - \frac{L_m\boldsymbol{\psi}_{rdq}^+}{\sigma L_sL_r}, \tag{6}$$

where $\sigma = (L_sL_r - L_m^2)/(L_sL_r)$.

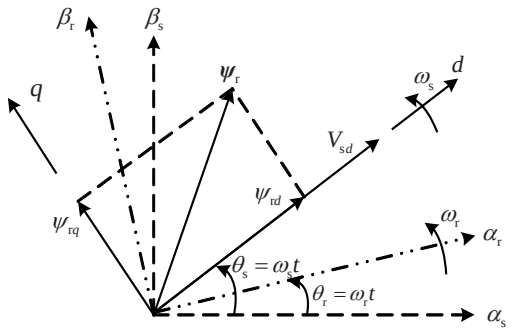

Fig.2 Phasor diagram of stator voltage orientation during balanced supply voltage

Thus, the stator output active and reactive powers can be calculated as

$$\begin{aligned} P_s + \mathrm{j}Q_s &= -\frac{3}{2}\boldsymbol{V}_{sdq}^+ \cdot \hat{\boldsymbol{I}}_{sdq}^+ = -\frac{3}{2}V_{sd}^+\left(\frac{\boldsymbol{\psi}_{sdq}^+}{\sigma L_s} - \frac{L_m\boldsymbol{\psi}_{rdq}^+}{\sigma L_sL_r}\right) \\ &= -\frac{3}{2}\frac{V_{sd}^+}{\sigma L_s}\left(\mathrm{j}\frac{V_{sd}^+}{\omega_s} - \frac{L_m}{L_r}(\psi_{rd}^+ - \mathrm{j}\psi_{rq}^+)\right). \end{aligned} \tag{7}$$

where $\hat{\boldsymbol{I}}_{sdq}^+$ is the conjugated space vector of $\boldsymbol{I}_{sdq}^+$.

Splitting Eq.(7) into real and imaginary parts yields

$$P_s = k_\sigma V_{sd}^+\psi_{rd}^+, \ Q_s = -k_\sigma V_{sd}^+\left(\frac{L_r}{L_m}\frac{V_{sd}^+}{\omega_s} + \psi_{rq}^+\right), \tag{8}$$

where $k_\sigma = \dfrac{3}{2}\dfrac{L_m}{\sigma L_sL_r}$.

Since the stator voltage remains constant during balanced network supply, according to Eq.(8), the active and reactive power changes over a constant period of sampling time T_s are given by

$$\Delta P_s = k_\sigma V_{sd}^+\Delta\psi_{rd}^+, \ \Delta Q_s = -k_\sigma V_{sd}^+\Delta\psi_{rq}^+. \tag{9}$$

At the beginning of the sampling period T_s, the active and reactive power errors are calculated as

$$\Delta P_s = P_s^* - P_s, \ \Delta Q_s = Q_s^* - Q_s. \tag{10}$$

Based on Eq.(9), in order to reduce the power errors in Eq.(10) to null, the rotor flux changes in the dq^+ reference frame must follow

$$\Delta\psi_{rd}^{+}=\frac{\Delta P_s}{k_\sigma V_{sd}^{+}},\quad \Delta\psi_{rq}^{+}=-\frac{\Delta Q_s}{k_\sigma V_{sd}^{+}}. \tag{11}$$

From Eq.(2b), the rotor flux can be calculated as

$$\frac{\mathrm{d}\boldsymbol{\psi}_{rdq}^{+}}{\mathrm{d}t}=\boldsymbol{V}_{rdq}^{+}-R_r\boldsymbol{I}_{rdq}^{+}-\mathrm{j}\omega_{slip+}\boldsymbol{\psi}_{rdq}^{+}. \tag{12}$$

Within the period of T_s, the rotor flux changes in the dq^+ reference frame are given by

$$\begin{cases}\Delta\psi_{rd}^{+}/T_s=V_{rd}^{+}-R_rI_{rd}^{+}+\omega_{slip+}\psi_{rq}^{+},\\ \Delta\psi_{rq}^{+}/T_s=V_{rq}^{+}-R_rI_{rq}^{+}-\omega_{slip+}\psi_{rd}^{+}.\end{cases} \tag{13}$$

Combining Eq.(11) with Eq.(13), the rotor voltages required to eliminate the power errors over the period of T_s are calculated as

$$\begin{cases}V_{rd}^{+}=\dfrac{1}{T_s}\dfrac{\Delta P_s}{k_\sigma V_{sd}^{+}}+R_rI_{rd}^{+}-\omega_{slip+}\psi_{rq}^{+},\\ V_{rq}^{+}=-\dfrac{1}{T_s}\dfrac{\Delta Q_s}{k_\sigma V_{sd}^{+}}+R_rI_{rq}^{+}+\omega_{slip+}\psi_{rd}^{+}.\end{cases} \tag{14}$$

The rotor fluxes in the dq^+ reference frame are calculated based on Eq.(8) as

$$\psi_{rd}^{+}=\frac{P_s}{k_\sigma V_{sd}^{+}},\ \psi_{rq}^{+}=-\frac{Q_s}{k_\sigma V_{sd}^{+}}-\frac{L_r}{L_m}\frac{V_{sd}^{+}}{\omega_s}. \tag{15}$$

Neglecting the rotor resistance, substituting Eq.(15) into Eq.(14) yields the required rotor voltage in the dq^+ reference frame

$$\begin{cases}V_{rd}^{+}=\dfrac{1}{T_s}\dfrac{\Delta P_s}{k_\sigma V_{sd}^{+}}+\omega_{slip+}\left(\dfrac{Q_s}{k_\sigma V_{sd}^{+}}+\dfrac{L_r}{L_m}\dfrac{V_{sd}^{+}}{\omega_s}\right),\\ V_{rq}^{+}=-\dfrac{1}{T_s}\dfrac{\Delta Q_s}{k_\sigma V_{sd}^{+}}+\omega_{slip+}\dfrac{P_s}{k_\sigma V_{sd}^{+}}.\end{cases} \tag{16}$$

As can be seen, calculations of the rotor voltage references require only simple multiplications and divisions without any integral operation.

Unbalanced network voltage

Assuming no zero sequence components exist, the three-phase quantities such as voltage, current and flux may be decomposed into positive and negative sequence components when the network voltage is unbalanced. As shown in Fig.3, for the positive dq^+ reference frame, the d^+-axis is fixed to the positive stator voltage V_{sd+}^{+} rotating at the speed of ω_s; while for the negative dq^- reference frame, its d^--axis rotates at the angular speed of $-\omega_s$ and with the phase angle $-\theta_s$ to the α_s-axis.

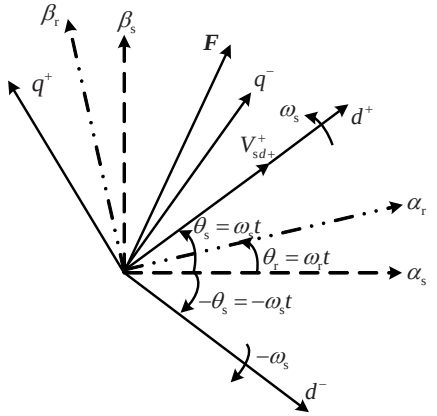

Fig.3 Phasor diagram of stator-voltage oriented with d^+-axis fixed to V_{sd+}^{+} during network voltage unbalance

According to Fig.3, the transformation between $(\alpha\beta)_s$, $(\alpha\beta)_r$ and dq^+ and dq^- reference frames are given by

$$\begin{cases}\boldsymbol{F}_{dq}^{+}=\boldsymbol{F}_{(\alpha\beta)_s}\mathrm{e}^{-\mathrm{j}\omega_s t},\ \boldsymbol{F}_{dq}^{-}=\boldsymbol{F}_{(\alpha\beta)_s}\mathrm{e}^{\mathrm{j}\omega_s t},\\ \boldsymbol{F}_{dq}^{+}=\boldsymbol{F}_{dq}^{-}\mathrm{e}^{-\mathrm{j}2\omega_s t},\ \boldsymbol{F}_{dq}^{-}=\boldsymbol{F}_{dq}^{+}\mathrm{e}^{\mathrm{j}2\omega_s t},\\ \boldsymbol{F}_{dq}^{+}=\boldsymbol{F}_{(\alpha\beta)_r}\mathrm{e}^{-\mathrm{j}2\omega_{slip+}t},\ \boldsymbol{F}_{dq}^{-}=\boldsymbol{F}_{(\alpha\beta)_r}\mathrm{e}^{\mathrm{j}2\omega_{slip-}t},\end{cases} \tag{17}$$

where F represents the voltage, current, or flux vector, the superscript '−' in $\boldsymbol{F}_{dq}^{-}$ represents the negative synchronously rotating reference frame, and $\omega_{slip-}=-\omega_s-\omega_r$.

According to Eq.(17) and Fig.3, the stator and rotor current, voltage, and flux vectors can be expressed in terms of their respective positive and negative sequence components in the positive and negative synchronous reference frames as

$$\boldsymbol{F}_{sdq}^{+}=\boldsymbol{F}_{sdq+}^{+}+\boldsymbol{F}_{sdq-}^{+}=\boldsymbol{F}_{sdq+}^{+}+\boldsymbol{F}_{sdq-}^{-}\mathrm{e}^{-\mathrm{j}2\omega_s t}. \tag{18}$$

Under unbalanced network conditions, the amplitude and rotating speed of the stator flux are no longer constant. Consequently, considering Eq.(18) and neglecting the voltage drop across the stator resistance, Eq.(2a) can be rearranged as

$$\boldsymbol{V}_{sdq}^{+} \approx \mathrm{j}\omega_s \boldsymbol{\psi}_{sdq}^{+} + \frac{\mathrm{d}\boldsymbol{\psi}_{sdq}^{+}}{\mathrm{d}t} = \mathrm{j}\omega_s \left(\boldsymbol{\psi}_{sdq+}^{+} - \boldsymbol{\psi}_{sdq-}^{-} \mathrm{e}^{-\mathrm{j}2\omega_s t}\right). \quad (19)$$

Hence, the following results can be obtained

$$\begin{cases} \psi_{sd+}^{+} = V_{sq+}^{+} / \omega_s, \quad \psi_{sq+}^{+} = -V_{sd+}^{+} / \omega_s, \\ \psi_{sd-}^{-} = -V_{sq-}^{-} / \omega_s, \quad \psi_{sq-}^{-} = V_{sd-}^{-} / \omega_s. \end{cases} \quad (20)$$

The stator current in the dq^+ reference frame can also be represented as

$$\begin{aligned} \boldsymbol{I}_{sdq}^{+} = \frac{\boldsymbol{\psi}_{sdq}^{+}}{\sigma L_s} - \frac{L_m \boldsymbol{\psi}_{rdq}^{+}}{\sigma L_s L_r} = \frac{\boldsymbol{\psi}_{sdq+}^{+} + \boldsymbol{\psi}_{sdq-}^{-} \mathrm{e}^{-\mathrm{j}2\omega_s t}}{\sigma L_s} \\ - \frac{L_m}{\sigma L_s L_r}\left(\boldsymbol{\psi}_{rdq+}^{+} + \boldsymbol{\psi}_{rdq-}^{-} \mathrm{e}^{-\mathrm{j}2\omega_s t}\right). \end{aligned} \quad (21)$$

Similar to the balanced voltage condition, the stator output active and reactive powers can be calculated by

$$P_s + \mathrm{j}Q_s = -\frac{3}{2}\boldsymbol{V}_{sdq}^{+} \cdot \hat{\boldsymbol{I}}_{sdq}^{+}. \quad (22)$$

Substituting Eqs.(19) and (21) into Eq.(22) and separating the active and reactive powers into different oscillating terms, yield

$$\begin{cases} P_s = P_{s0} + P_{s\sin 2} \sin(2\omega_s t) + P_{s\cos 2} \cos(2\omega_s t), \\ Q_s = Q_{s0} + Q_{s\sin 2} \sin(2\omega_s t) + Q_{s\cos 2} \cos(2\omega_s t), \end{cases} \quad (23)$$

where

$$\begin{bmatrix} P_{s0} \\ Q_{s0} \\ P_{s\sin 2} \\ P_{s\cos 2} \\ Q_{s\sin 2} \\ Q_{s\cos 2} \end{bmatrix} = \frac{3\omega_s}{2\sigma L_s} \begin{bmatrix} 0 & 0 & 0 & 0 \\ -\psi_{sd+}^{+} & -\psi_{sq+}^{+} & \psi_{sd-}^{-} & \psi_{sq-}^{-} \\ \psi_{sd-}^{-} & \psi_{sq-}^{-} & \psi_{sd+}^{+} & \psi_{sq+}^{+} \\ -\psi_{sq-}^{-} & \psi_{sd-}^{-} & \psi_{sq+}^{+} & -\psi_{sd+}^{+} \\ 0 & 0 & 0 & 0 \\ 0 & 0 & 0 & 0 \end{bmatrix} \begin{bmatrix} V_{sq+}^{+} \\ -V_{sd+}^{+} \\ -V_{sq-}^{-} \\ V_{sd-}^{-} \end{bmatrix}$$

$$+ \frac{3}{2}\frac{\omega_s L_m}{\sigma L_s L_r} \begin{bmatrix} -\psi_{sq+}^{+} & \psi_{sd+}^{+} & \psi_{sq-}^{-} & -\psi_{sd-}^{-} \\ \psi_{sd+}^{+} & \psi_{sq+}^{+} & -\psi_{sd-}^{-} & -\psi_{sq-}^{-} \\ -\psi_{sd-}^{-} & -\psi_{sq-}^{-} & -\psi_{sd+}^{+} & -\psi_{sq+}^{+} \\ \psi_{sq-}^{-} & -\psi_{sd-}^{-} & -\psi_{sq+}^{+} & \psi_{sd+}^{+} \\ -\psi_{sq-}^{-} & \psi_{sd-}^{-} & -\psi_{sq+}^{+} & \psi_{sd+}^{+} \\ -\psi_{sd-}^{-} & -\psi_{sq-}^{-} & \psi_{sd+}^{+} & \psi_{sq+}^{+} \end{bmatrix} \begin{bmatrix} \psi_{rd+}^{+} \\ \psi_{rq+}^{+} \\ \psi_{rd-}^{-} \\ \psi_{rq-}^{-} \end{bmatrix}. \quad (24)$$

Considering Eq.(20) and with V_{sd+}^{+} fixed to the d^+-axis, as shown in Fig.3, Eq.(24) can be simplified as

$$\begin{aligned} &\frac{2}{3}\sigma L_s \begin{bmatrix} P_{s0} \\ Q_{s0} \\ P_{s\sin 2} \\ P_{s\cos 2} \\ Q_{s\sin 2} \\ Q_{s\cos 2} \end{bmatrix} - \frac{1}{\omega_s} \begin{bmatrix} 0 \\ -(V_{sd+}^{+})^2 + (V_{sq-}^{-})^2 + (V_{sd-}^{-})^2 \\ -2V_{sd-}^{-}V_{sd+}^{+} \\ 2V_{sq-}^{-}V_{sd+}^{+} \\ 0 \\ 0 \end{bmatrix} \\ &= \frac{L_m}{L_r} \begin{bmatrix} V_{sd+}^{+} & 0 & V_{sd-}^{-} & V_{sq-}^{-} \\ 0 & -V_{sd+}^{+} & V_{sq-}^{-} & -V_{sd-}^{-} \\ V_{sq-}^{-} & -V_{sd-}^{-} & 0 & V_{sd+}^{+} \\ V_{sd-}^{-} & V_{sq-}^{-} & V_{sd+}^{+} & 0 \\ -V_{sd-}^{-} & -V_{sq-}^{-} & V_{sd+}^{+} & 0 \\ V_{sq-}^{-} & -V_{sd-}^{-} & 0 & -V_{sd+}^{+} \end{bmatrix} \begin{bmatrix} \psi_{rd+}^{+} \\ \psi_{rq+}^{+} \\ \psi_{rd-}^{-} \\ \psi_{rq-}^{-} \end{bmatrix}. \end{aligned} \quad (25)$$

With $P_{s\sin 2}$=$P_{s\cos 2}$=0 set for the system control target during network unbalance, the required rotor fluxes in the dq^+ and dq^- reference frames can be calculated as

$$\begin{cases} \psi_{rd+}^{+} = \dfrac{2}{3}\dfrac{\sigma L_s L_r V_{sd+}^{+}}{L_m D_2} P_{s0}, \\ \psi_{rq+}^{+} = -\dfrac{L_r V_{sd+}^{+} D_3}{L_m D_1} - \dfrac{2L_r V_{sd+}^{+}}{D_1 \omega_s L_m}[(V_{sd-}^{-})^2 + (V_{sq-}^{-})^2], \\ \psi_{rd-}^{-} = -\dfrac{2L_r V_{sq-}^{-}}{\omega_s L_m} - k_{dd}\psi_{rd+}^{+} - k_{qd}\psi_{rq+}^{+}, \\ \psi_{rq-}^{-} = \dfrac{2L_r V_{sd-}^{-}}{\omega_s L_m} - k_{qd}\psi_{rd+}^{+} + k_{dd}\psi_{rq+}^{+}, \end{cases} \quad (26)$$

where

$$D_1 = (V_{sd+}^{+})^2 + (V_{sd-}^{-})^2 + (V_{sq-}^{-})^2,$$

$$D_2 = (V_{sd+}^{+})^2 - [(V_{sd-}^{-})^2 + (V_{sq-}^{-})^2],$$

$$D_3 = \frac{2}{3}\sigma L_s Q_{s0} + [(V_{sd+}^{+})^2 - (V_{sd-}^{-})^2 - (V_{sq-}^{-})^2] / \omega_s,$$

$$k_{dd} = V_{sd-}^{-} / V_{sd+}^{+}, \quad k_{qd} = V_{sq-}^{-} / V_{sd+}^{+}.$$

Similarly, according to Eq.(26), the rotor flux changes can be expressed as

$$\begin{cases}\dfrac{\mathrm{d}}{\mathrm{d}t}\psi^{+}_{\mathrm{r}d+}=\dfrac{2\sigma L_{\mathrm{s}}L_{\mathrm{r}}V^{+}_{\mathrm{s}d+}}{3L_{\mathrm{m}}D_2}\dfrac{\mathrm{d}}{\mathrm{d}t}P_{\mathrm{s}0},\\ \dfrac{\mathrm{d}}{\mathrm{d}t}\psi^{+}_{\mathrm{r}q+}=-\dfrac{2\sigma L_{\mathrm{s}}L_{\mathrm{r}}V^{+}_{\mathrm{s}d+}}{3L_{\mathrm{m}}D_1}\dfrac{\mathrm{d}}{\mathrm{d}t}Q_{\mathrm{s}0},\\ \dfrac{\mathrm{d}}{\mathrm{d}t}\psi^{-}_{\mathrm{r}d-}=-k_{dd}\dfrac{\mathrm{d}}{\mathrm{d}t}\psi^{+}_{\mathrm{r}d+}-k_{qd}\dfrac{\mathrm{d}}{\mathrm{d}t}\psi^{+}_{\mathrm{r}q+},\\ \dfrac{\mathrm{d}}{\mathrm{d}t}\psi^{-}_{\mathrm{r}q-}=-k_{qd}\dfrac{\mathrm{d}}{\mathrm{d}t}\psi^{+}_{\mathrm{r}d+}+k_{dd}\dfrac{\mathrm{d}}{\mathrm{d}t}\psi^{+}_{\mathrm{r}q+}.\end{cases}\tag{27}$$

Over a constant period of time T_{s}, the flux changes are given by

$$\begin{cases}\Delta\psi^{+}_{\mathrm{r}d+}=\dfrac{2\sigma L_{\mathrm{s}}L_{\mathrm{r}}V^{+}_{\mathrm{s}d+}}{3L_{\mathrm{m}}D_2}\Delta P_{\mathrm{s}0},\\ \Delta\psi^{+}_{\mathrm{r}q+}=-\dfrac{2\sigma L_{\mathrm{s}}L_{\mathrm{r}}V^{+}_{\mathrm{s}d+}}{3L_{\mathrm{m}}D_1}\Delta Q_{\mathrm{s}0},\\ \Delta\psi^{-}_{\mathrm{r}d-}=-k_{dd}\Delta\psi^{+}_{\mathrm{r}d+}-k_{qd}\Delta\psi^{+}_{\mathrm{r}q+},\\ \Delta\psi^{-}_{\mathrm{r}q-}=-k_{qd}\Delta\psi^{+}_{\mathrm{r}d+}+k_{dd}\Delta\psi^{+}_{\mathrm{r}q+}.\end{cases}\tag{28}$$

Similar to Eq.(14), during network unbalance the required rotor voltage in the dq^{+} and dq^{-} reference frames can be calculated by

$$\begin{cases}V^{+}_{\mathrm{r}d+}=\dfrac{\mathrm{d}}{\mathrm{d}t}\psi^{+}_{\mathrm{r}d+}+R_{\mathrm{r}}I^{+}_{\mathrm{r}d+}-\omega_{\mathrm{slip}+}\psi^{+}_{\mathrm{r}q+},\\ V^{+}_{\mathrm{r}q+}=\dfrac{\mathrm{d}}{\mathrm{d}t}\psi^{+}_{\mathrm{r}q+}+R_{\mathrm{r}}I^{+}_{\mathrm{r}q+}+\omega_{\mathrm{slip}+}\psi^{+}_{\mathrm{r}d+},\\ V^{-}_{\mathrm{r}d-}=\dfrac{\mathrm{d}}{\mathrm{d}t}\psi^{-}_{\mathrm{r}d-}+R_{\mathrm{r}}I^{-}_{\mathrm{r}d-}-\omega_{\mathrm{slip}-}\psi^{-}_{\mathrm{r}q-},\\ V^{-}_{\mathrm{r}q-}=\dfrac{\mathrm{d}}{\mathrm{d}t}\psi^{-}_{\mathrm{r}q-}+R_{\mathrm{r}}I^{-}_{\mathrm{r}q-}+\omega_{\mathrm{slip}-}\psi^{-}_{\mathrm{r}d-}.\end{cases}\tag{29}$$

With the constant period of time T_{s} and neglecting the rotor resistance, Eq.(29) can be rewritten as

$$\begin{cases}V^{+}_{\mathrm{r}d+}=\Delta\psi^{+}_{\mathrm{r}d+}/T_{\mathrm{s}}-\omega_{\mathrm{slip}+}\psi^{+}_{\mathrm{r}q+},\\ V^{+}_{\mathrm{r}q+}=\Delta\psi^{+}_{\mathrm{r}q+}/T_{\mathrm{s}}+\omega_{\mathrm{slip}+}\psi^{+}_{\mathrm{r}d+},\\ V^{-}_{\mathrm{r}d-}=\Delta\psi^{-}_{\mathrm{r}d-}/T_{\mathrm{s}}-\omega_{\mathrm{slip}-}\psi^{-}_{\mathrm{r}q-},\\ V^{-}_{\mathrm{r}q-}=\Delta\psi^{-}_{\mathrm{r}q-}/T_{\mathrm{s}}+\omega_{\mathrm{slip}-}\psi^{-}_{\mathrm{r}d-},\end{cases}\tag{30}$$

where $\psi^{+}_{\mathrm{r}d+}$, $\psi^{+}_{\mathrm{r}q+}$, $\psi^{-}_{\mathrm{r}d-}$, $\psi^{-}_{\mathrm{r}q-}$ and $\Delta\psi^{+}_{\mathrm{r}d+}$, $\Delta\psi^{+}_{\mathrm{r}q+}$, $\Delta\psi^{-}_{\mathrm{r}d-}$, $\Delta\psi^{-}_{\mathrm{r}q-}$ can be obtained according to Eqs.(26) and (28), respectively.

Finally, the required rotor voltage in the dq^{+} and dq^{-} reference frames can be calculated by

$$\begin{cases}V^{+}_{\mathrm{r}d+}=\dfrac{1}{T_{\mathrm{s}}}\dfrac{2\sigma L_{\mathrm{s}}L_{\mathrm{r}}V^{+}_{\mathrm{s}d+}}{3L_{\mathrm{m}}D_2}\Delta P_{\mathrm{s}0}-\omega_{\mathrm{slip}+}\left(-\dfrac{L_{\mathrm{r}}V^{+}_{\mathrm{s}d+}D_3}{L_{\mathrm{m}}D_1}\right.\\ \qquad\left.-\dfrac{2L_{\mathrm{r}}V^{+}_{\mathrm{s}d+}}{D_1\omega_{\mathrm{s}}L_{\mathrm{m}}}\left((V^{-}_{\mathrm{s}d-})^2+(V^{-}_{\mathrm{s}q-})^2\right)\right),\\ V^{+}_{\mathrm{r}q+}=-\dfrac{1}{T_{\mathrm{s}}}\dfrac{2\sigma L_{\mathrm{s}}L_{\mathrm{r}}V^{+}_{\mathrm{s}d+}}{3L_{\mathrm{m}}D_1}\Delta Q_{\mathrm{s}0}+\omega_{\mathrm{slip}+}\cdot\dfrac{2}{3}\dfrac{\sigma L_{\mathrm{s}}L_{\mathrm{r}}V^{+}_{\mathrm{s}d+}}{L_{\mathrm{m}}D_2}P_{\mathrm{s}0},\\ V^{-}_{\mathrm{r}d-}=-\dfrac{1}{T_{\mathrm{s}}}\left(k_{dd}\Delta\psi^{+}_{\mathrm{r}d+}+k_{qd}\Delta\psi^{+}_{\mathrm{r}q+}\right)\\ \qquad-\omega_{\mathrm{slip}-}\left(2L_{\mathrm{r}}V^{-}_{\mathrm{s}d-}/(\omega_{\mathrm{s}}L_{\mathrm{m}})-k_{qd}\psi^{+}_{\mathrm{r}d+}+k_{dd}\psi^{+}_{\mathrm{r}q+}\right),\\ V^{-}_{\mathrm{r}q-}=-\dfrac{1}{T_{\mathrm{s}}}\left(k_{qd}\Delta\psi^{+}_{\mathrm{r}d+}-k_{dd}\Delta\psi^{+}_{\mathrm{r}q+}\right)\\ \qquad+\omega_{\mathrm{slip}-}\left(-2L_{\mathrm{r}}V^{-}_{\mathrm{s}q-}/(\omega_{\mathrm{s}}L_{\mathrm{m}})-k_{dd}\psi^{+}_{\mathrm{r}d+}-k_{qd}\psi^{+}_{\mathrm{r}q+}\right).\end{cases}\tag{31}$$

It is worth noting that, compared with the required rotor voltages output from the dual-PI rotor current regulators in (Xu and Wang, 2007; Hu *et al*., 2007), the calculations of rotor voltage references by using the proposed DPC during the network voltage unbalance require only simple operations of multiplication and division. In particular, the decomposition process of the positive and negative sequence rotor currents, which is essential in dual-PI rotor current regulators, is totally eliminated.

Finally, the rotor control voltage will be transformed into the rotor reference $(\alpha\beta)_{\mathrm{r}}$ frame as

$$\boldsymbol{V}_{(\alpha\beta)_{\mathrm{r}}}=\boldsymbol{V}^{+}_{\mathrm{r}dq+}\mathrm{e}^{\mathrm{j}(\theta_{\mathrm{s}}-\theta_{\mathrm{r}})}+\boldsymbol{V}^{-}_{\mathrm{r}dq-}\mathrm{e}^{-\mathrm{j}(\theta_{\mathrm{s}}+\theta_{\mathrm{r}})}.\tag{32}$$

SYSTEM IMPLEMENTATION

The schematic diagram of the conventional DPC strategy is shown in Fig.4. Three-phase stator voltages and currents are measured and transformed into a stationary $(\alpha\beta)_{\mathrm{s}}$ reference frame. A phase-locked loop (PLL) is used to detect the stator voltage angle θ_{s} and its rotating angular speed ω_{s}. After stator output active and reactive powers being calculated, the

required rotor voltage in the dq^+ reference frame is predicated using Eq.(16) and transformed into the rotor reference frame using the rotor slip angle obtained from a shaft encoder. Finally, the space vector modulation (SVM) technique is used to obtain switching patterns to control the rotor side converter (RSC) with a constant switching frequency.

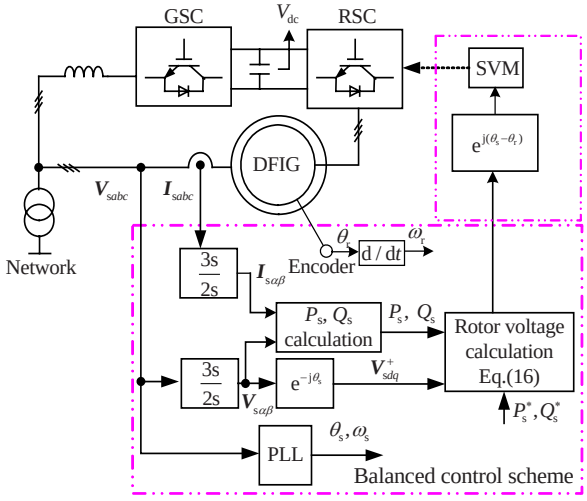

Fig.4 Scheme of the conventional DPC for a DFIG system

Under unbalanced network conditions, stator voltage contains both positive and negative sequence components. To achieve accurate dq^+ and dq^- reference frame transformations, the PLL must lock to the positive sequence stator voltage. Various methods have been reported in the literature and the scheme adopted here is to use a notch filter tuned at twice the line frequency to remove the negative sequence components, as shown in Fig.5. The required positive and negative sequence rotor voltages in the dq^+ and dq^- reference frames are calculated using Eq.(31), and then transformed into the rotor reference frame using Eq.(32). Finally, the schematic diagram of the overall control system with the proposed DPC strategy applied under unbalanced network conditions is shown in Fig.6.

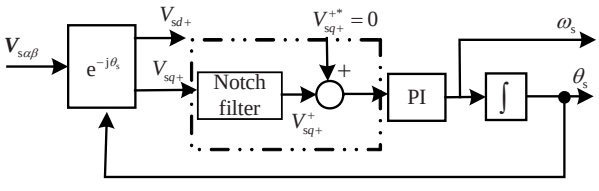

Fig.5 Schematic diagram of the phase-locked loop (PLL)

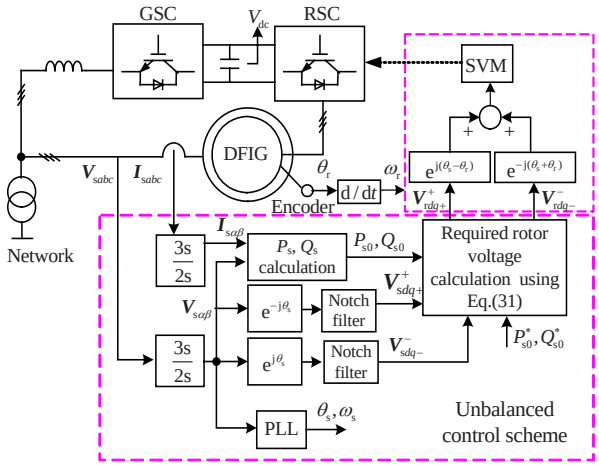

Fig.6 Scheme of the proposed DPC for a DFIG system

SIMULATION STUDIES

Simulations of the proposed DPC strategy for a DFIG-based wind power generation system were conducted using PSCAD/EMTDC. The DFIG was rated at 2 MW with parameters listed in Table 1. Fig.7 shows the schematic diagram of the simulated system. A single-phase load at the primary side of the coupling transformer was used to generate the voltage unbalance. The nominal DC link voltage was set at 1 200 V and the switching frequencies for both converters were 2 000 Hz. The main target of the grid side converter was assigned to control the DC link voltage with the similar method used in (Song and Nam, 1999; Hu *et al*., 2007). As shown in Fig.7, a high frequency AC filter is shunt-connected to the stator side to absorb the switching harmonics generated by the two converters.

Initial studies with various active and reactive power steps were carried out to test the dynamic response using the conventional control scheme shown in Fig.4 in the conditions of balanced supply voltage. First, the DFIG was assumed to be in speed control, viz., the rotor speed was set externally, as the large inertia of the wind turbine resulting in a slow change of the rotor speed. The simulation results are shown in Fig.8a with the rotor speed fixed at 1.2 p.u. The active and reactive powers were initially set at 0 MW and −0.5 MV·A, respectively, where '−' refers to absorbing reactive power. Various power steps were applied, viz., active and reactive power references were changed from 0 to −2 MW at the instant of 1.3 s,

Table 1 Parameters of the simulated DFIG

Parameter	Value
Rated power	2 MW
Stator voltage	690 V/50 Hz
Stator/rotor turns ratio	0.3
Stator resistance R_s	0.010 8 p.u.
Rotor resistance R_r	0.012 1 p.u.*
Mutual inductance L_m	3.362 p.u.
Stator leakage inductance $L_{\sigma s}$	0.102 p.u.
Rotor leakage inductance $L_{\sigma r}$	0.110 p.u.*
Lumped inertia constant	0.4 s
Number of pole pairs	2

* Referred to the stator

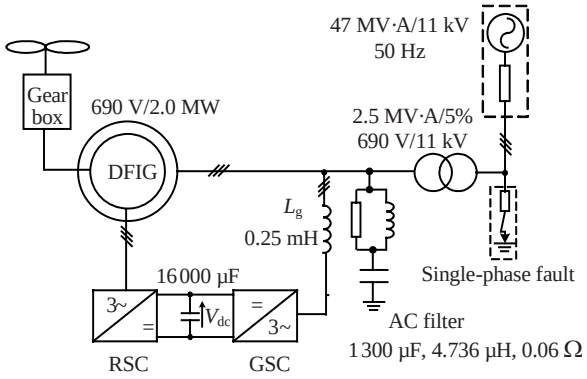

Fig.7 Schematic diagram of the tested system

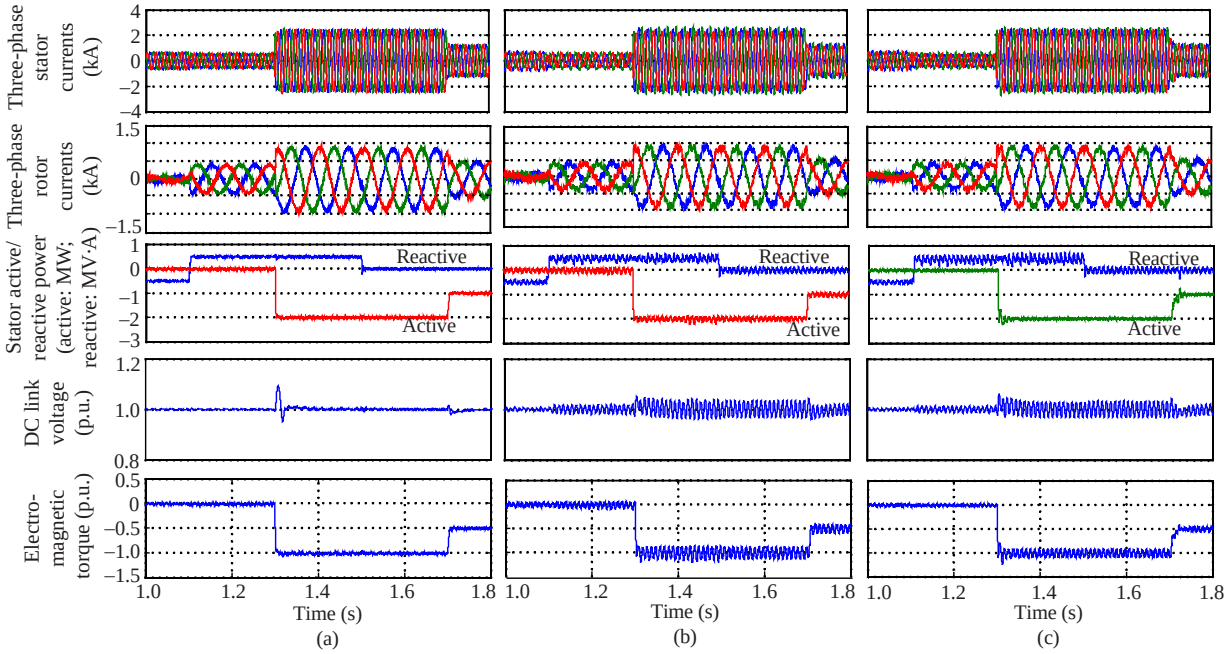

Fig.8 Simulation results under various stator active and reactive power steps with the rotor speed fixed at 1.2 p.u.
(a) Conventional DPC under balanced supply voltage; (b) Conventional DPC under 5% unbalanced supply voltage; (c) Proposed DPC under 5% unbalanced supply voltage

to −1 MW at 1.7 s, and from −0.5 MV·A to 0.5 MV·A at 1.1 s, to 0 at 1.5 s, respectively. The effectiveness of the conventional control scheme is clearly indicated in Fig.8a. The dynamic responses of both active and reactive powers are within a few milliseconds and without overshoot either in the active/reactive powers or in the stator/rotor currents, which behaves identically to that in (Zhi and Xu, 2007).

Studies under the same operating conditions as given in Fig.8a were conducted during 5% network voltage unbalance. The results are shown in Fig.8b. It is obvious that, under unbalanced network conditions, the system performance using the conventional control scheme in Fig.4 was degraded with high stator and rotor current unbalances, as shown in the first two subfigures of Fig.8b. Significant oscillations (100 Hz, twice the line frequency) appeared in the stator output active/reactive powers and generator's electromagnetic torque, as shown in the third and fifth subfigures of Fig.8b. The three-phase rotor currents, whose frequency equals the rotor mechanical frequency minus the stator frequency, contained both the fundamental component of 10 Hz (i.e., 60−50) and the harmonic component of 110 Hz (i.e., 60+50). The measured stator current unbalance was around 3.2% and the amplitude of the rotor 110 Hz current harmonic was about 6.9% of the fundamental component of 10 Hz. The oscillations of the stator active/reactive

powers and electromagnetic torque were ±5.5%, ±5.9% and ±12.5% of their respective rated values.

As expressed in Eq.(3), Eq.(16) and Fig.4, since the negative sequence components are not taken into account in the conventional DPC scheme, the 100 Hz oscillations in either the active or the reactive power cannot be controlled or eliminated during supply voltage unbalance. For comparison, Fig.8c shows the results with the proposed control scheme in Fig.6 employed under the condition of 5% stator voltage unbalance. Since $P_{s\sin 2}$=0 and $P_{s\cos 2}$=0 were both set for system control, the stator active power oscillations were effectively eliminated, as shown in the third subfigure of Fig.8c. Meanwhile, the stator and rotor current unbalances were diminished as well. For a clear illustration, the measured stator current unbalance, the rotor relative amplitude of 110 Hz to the fundamental 10 Hz component, and the pulsations of the stator active/reactive powers and electromagnetic torque at twice the line frequency, are all summarized in Table 2. From the third subfigure of Fig.8c and Table 2, it can be concluded that the system performance predicted by the proposed control scheme is satisfactory with stator output active power pulsations fully eliminated.

Similar tests have also been carried out for different rotor speeds, and the system performances were found to be identical to those shown in Fig.8. Due to space limitation, they are not shown here.

As shown in the fourth subfigures of Figs.8b and 8c, with the conventional and the proposed DPC schemes, the DC link voltage contains 100 Hz oscillations, since the active power exchange between the DFIG and the rotor side converter contains 100 Hz oscillations with unbalanced network voltage. However, the impact of such oscillations on the system operation is found to be negligible as the control target illustrated in Fig.6 was fully achieved, as shown in the third subfigure of Fig.8c.

Further tests with the DFIG being torque controlled were carried out and the simulation results are shown in Fig.9. The DFIG was operated in the maximal power-tracking mode where its active power/torque was controlled according to the optimal speed curve depicted in Fig.10 (Gagnon *et al*., 2005). This characteristic is illustrated by the *ABCD* curve superimposed on the mechanical power characteristics of the turbine obtained at different wind speeds. The actual speed ω_r of the turbine was measured, and the corresponding mechanical power of the tracking characteristic was used as the active reference power. Four points *A*, *B*, *C* and *D* define the tracking characteristic. From zero speed to the speed of point *A*, the reference power is zero. Between points *A* and *B*, the tracking characteristic is a straight line. Between points *B* and *C*, the tracking characteristic is the locus of the maximum power of the turbine (maxima of the turbine power corresponding to the turbine speed curves). The tracking characteristic is a straight line from points *C* to *D*. The power at point *D* is 1 p.u., and beyond point *D* the reference power is a constant equal to 1 p.u.

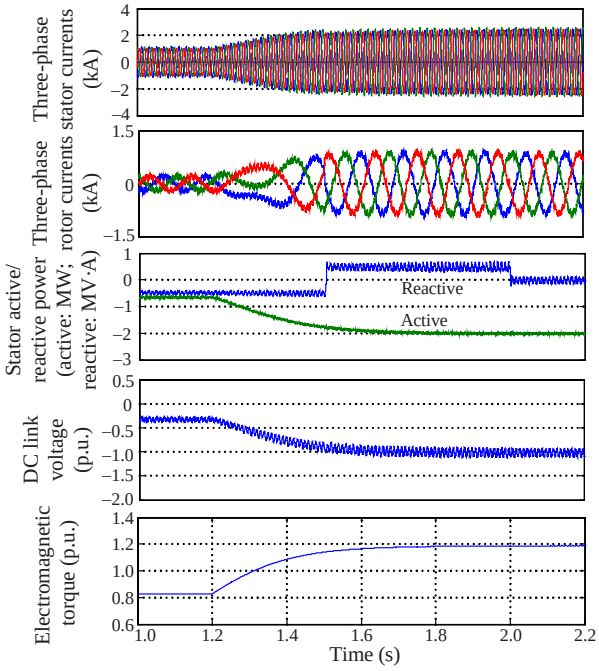

Fig.9 Simulation results with the proposed control scheme during speed and torque variations under 5% voltage unbalance

Table 2 Comparison between the conventional and the proposed control schemes during network voltage unbalance

Control scheme	I_s unbalance (%)	I_r 110 Hz harmonics (%)	P_s pulsations (%)	Q_s pulsations (%)	T_e pulsations (%)
Conventional	3.2	6.9	±5.5	±5.9	±12.5
Proposed	2.6	5.6	±0.1	±6.1	±6.5

$\boldsymbol{I}_s$ and $\boldsymbol{I}_r$ represent stator and rotor current vectors, respectively; $\boldsymbol{T}_e$ is electromagnetic torque

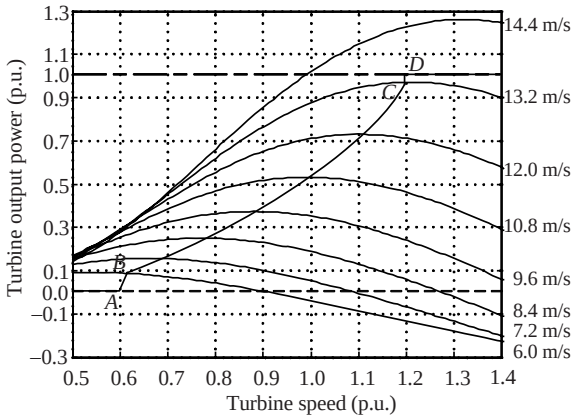

Fig.10 Turbine and tracking characteristics with the pitch angle β=0°. Points *A*, *B*, *C* and *D* define the tracking characteristic

As shown in Fig.9, the wind speed is step changed from 9.6 m/s to 13.6 m/s at 1.2 s and the associated active power changed from 0.37 p.u. to 1.0 p.u. accordingly. The reactive power reference is stepped from −0.5 MV·A to 0.5 MV·A at 1.5 s and then to 0 at 2.0 s. In this test, the lumped inertia constant of the system was set to a relatively small value of 0.4 s for a clear illustration. It can be concluded from Fig.9 that the DFIG generation system operates satisfactorily during speed and power variations without any oscillations in the stator output active power.

CONCLUSION

This paper has proposed an analysis and an improved DPC design for a DFIG-based wind power generation system during network voltage unbalance. Simulation results were presented to demonstrate the feasibility of the proposed control scheme. Conclusions can be drawn as follows:

(1) The conventional DPC scheme without network unbalance considered can provide pretty good dynamic system performance when the supply voltage is strictly balanced. However, once the network is slightly unbalanced, the performance deteriorates with high stator/rotor current unbalances and significant oscillations in the stator active/reactive power and electromagnetic torque.

(2) The proposed DPC scheme, which is implemented in the SVO positive dq^+ and negative dq^- reference frames, gets rid of the decomposition process of positive and negative sequence rotor currents in the vector control scheme using dual-PI rotor current regulators. Besides, the system performance is enhanced by the elimination of the stator output active power oscillations and the reduction of the electromagnetic torque pulsations during network unbalance.

References

Chomat, M., Bendl, J., Schreier, L., 2002. Extended Vector Control of Doubly Fed Machine Under Unbalanced Power Network Conditions. Proc. IEEE Int. Conf. on Power Electronics, Machines and Drives, p.329-334. [doi:10.1049/cp:20020138]

Gagnon, R., Sybille, G., Bernard, S., Pare, D., Casoria, S., Larose, C., 2005. Modeling and Real-time Simulation of a Doubly-fed Induction Generator Driven by a Wind Turbine. Int. Conf. on Power Systems Transients, Montreal, Canada.

Gokhale, K.P., Karraker, D.W., Heikkila, S.J., 2002. Controller for a Wound Rotor Slip Ring Induction Machine. U.S. Patent, No. 6 448 735 B1.

Hu, J.B., He, Y.K., 2008. Reinforced control and operation of DFIG-based wind power generation system under unbalanced grid voltage conditions. *IEEE Trans. on Energy Conv.*, in press.

Hu, J.B., He, Y.K., Nian, H., 2007. Enhanced control of DFIG-used back-to-back PWM VSC under unbalanced grid voltage conditions. *J. Zhejiang Univ. Sci. A*, **8**(8):1330-1339. [doi:10.1631/jzus.2007.A1330]

Jang, J., Kim, Y., Lee, D., 2006. Active and Reactive Power Control of DFIG for Wind Energy Conversion Under Unbalanced Grid Voltage. CES/IEEE 5th Int. Power Electronics and Motion Control Conf., p.1-5. [doi:10.1109/IPEMC.2006.297323]

Pena, R., Clare, J.C., Asher, G.M., 1996. Doubly fed induction generator using back-to-back PWM converters and its application to variable-speed wind-energy generation. *IEEE Proc.-Electr. Power Appl.*, **143**(3):231-241. [doi:10.1049/ip-epa:19960288]

Pena, R., Crdenas, R., Escobar, E., Clare, J., Wheeler, P., 2007. Control system for unbalanced operation of stand-alone doubly fed induction generators. *IEEE Trans. on Energy Conv.*, **22**(2):544-545. [doi:10.1109/TEC.2007.895393]

Song, H.S., Nam, K., 1999. Dual current control scheme for PWM converter under unbalanced input voltage conditions. *IEEE Trans. on Ind. Electron.*, **46**(5):953-959. [doi:10.1109/41.793344]

Xu, L., Cartwright, P., 2006. Direct active and reactive power control of DFIG for wind energy generation. *IEEE Trans. on Energy Conv.*, **21**(3):750-758. [doi:10.1109/TEC.2006.875472]

Xu, L., Wang, Y., 2007. Dynamic modeling and control of DFIG based wind turbines under unbalanced network conditions. *IEEE Trans. on Power Syst.*, **22**(1):314-323. [doi:10.1109/TPWRS.2006.889113]

Zhi, D., Xu, L., 2007. Direct power control of DFIG with constant switching frequency and improved transient performance. *IEEE Trans. on Energy Conv.*, **22**(1):110-118. [doi:10.1109/TEC.2006.889549]

Zhou, Y., Bauer, P., Ferreira, J.A., Pierik, J., 2007. Control of DFIG Under Unsymmetrical Voltage Dip. IEEE Power Electronics Specialists Conf., p.933-938. [doi:10.1109/PESC.2007.4342113]